Dynamics of an Antenna Pointing Control System with Flexible Structures

Masazumi Ueba*
Nippon Telegraph and Telephone Corporation, Yokosuka 238-03, Japan

This paper describes the dynamics of an antenna pointing control system with flexible structures for multibeam communication satellites. The flexible structures are a large antenna main reflector and a subreflector support boom. The main reflector is connected to a rigid main body at multiple points and therefore constitutes a closed loop, and the support boom has a drive mechanism on its tip. First, the dynamics are derived by using Newton-Euler and constraint equations based on connection conditions and Lagrange multipliers and then clarified by incorporating the flexibility of the antenna main reflector and the support boom into coupling coefficients. Those coefficients are numerically and experimentally verified. Also, the effect of the critical structural parameters on the antenna pointing control system is evaluated.

Nomenclature

$(\boldsymbol{a}\times)$	= outer product of vector $\boldsymbol{a}$
C	= generalized mass of antenna support boom modified by driven subreflector
C_A^S	= coordinate transformation matrix from antenna main reflector to main body
E	= unit matrix (3×3)
E_R	= relative young modulus of beam AB
F_A	= force applied to antenna main reflector
F_S	= force applied to satellite main body
G_R	= relative modulus of rigidity of beam AB
H	= angular modal momentum of model Fig. 4 with respect to O_A
H_A	= angular modal momentum of antenna main reflector with respect to O_A
H_∞	= angular modal momentum of model Fig. 3 with respect to O_A
I_A	= moment of inertia of antenna main reflector
I_{AS}	= moment of inertia of antenna subreflector about driving center
I_e	= moment of inertia of experimental apparatus
I_S	= moment of inertia of satellite
J	= moment of inertia of the whole satellite including antenna main reflector
K_B	= antenna subreflector drive ratio
K_V, K_E	= ratio of beam angle to main reflector and subreflector vibration, respectively
k_p	= bearing stiffness of antenna pointing mechanism
m	= number of modes
m_A	= mass of antenna main reflector
m_S	= mass of satellite main body
P_A	= modal momentum of antenna main reflector
Q_A	= generalized force of antenna main reflector
$\boldsymbol{R}$	= distance between the origin of satellite main body and that of antenna main reflector
r_{Ag}	= center of gravity of antenna main reflector
r_{Ai}	= position of point i in the coordinate of antenna main reflector $(i = A,B)$
r_{Si}	= position of point i in the coordinate of satellite main body $(i = A,B)$
T_A	= torque applied to antenna main reflector
T_{AS}	= torque applied to antenna subreflector
T_e	= torque applied to rotating table
T_S	= torque applied to satellite main body
v_A	= velocity of antenna main reflector
v_S	= velocity of satellite main body
γ	= equivalent drive angle factor (= reflector angle/reflector displacement)
ζ_A	= damping ratio of antenna main reflector
ζ_{ASB}	= damping ratio of antenna support boom
ζ_P	= damping ratio of solar paddle
θ_{AS}	= antenna drive angle
θ_B	= beam pointing angle
θ_e	= rotational angle of rotating table
θ_S	= satellite attitude error
λ_1, λ_2	= Lagrange multipliers
ξ_A	= modal coordinate of antenna main reflector
ξ_{ASB}	= modal coordinate of antenna support boom
ξ_e	= modal coordinate of aluminum beam
ξ_p	= modal coordinate of solar paddle
$\sigma(i)$	= modal slope of point i
Φ_{AS}	= modal displacement of antenna subreflector
Φ'_{AS}	= modal slope of antenna subreflector
$\phi(i)$	= modal displacement of point i
Ω_A	= modal angular momentum of antenna main reflector with respect to O_S
Ω_{AS}	= flexible coupling of antenna subreflector
Ω_{ASB}	= modal angular momentum of antenna support boom and driven subreflector
Ω_e	= coupling coefficient of experimental apparatus
Ω_p	= modal angular momentum of solar paddle
Ω_R	= rigid coupling of antenna subreflector
ω_A	= angular velocity vector of antenna main reflector
ω_{AMA}	= eigenfrequency of antenna main reflector
ω_{ASB}	= eigenfrequency of antenna support boom
ω_e	= eigenfrequency of aluminum beam
ω_p	= eigenfrequency of solar paddle
ω_s	= angular velocity vector of satellite main body

Received June 28, 1990; presented as Paper 90-2951 at the AIAA/AAS Astrodynamics Conference, Portland, OR, Aug. 20–22, 1990; revision received Jan. 4, 1991; accepted for publication Jan. 5, 1991.

*Research Engineer, Radio Communication Systems Laboratories, 1-2356 Take Yokosuka-shi Kanagawa.

Introduction

FOR next-generation satellite communications, multibeam systems are the most promising. In such systems, it is necessary for the beam pointing direction of large onboard antennas to be accurately controlled because of their narrow beam width. To design a control system with higher antenna pointing accuracy, it is important to clarify the satellite dynamics of large flexible antennas.

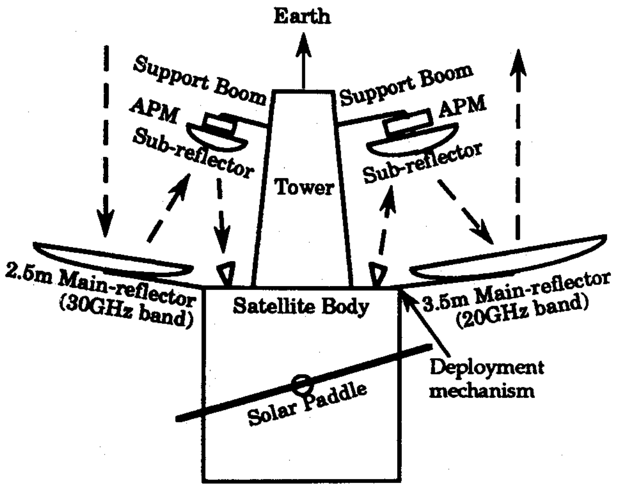

Fig. 1 Antenna system configuration.

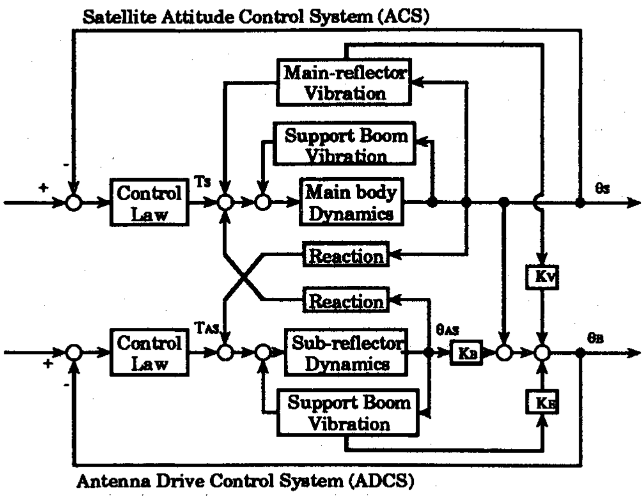

Fig. 2 Block diagram of the antenna pointing control system.

Orbital experiments are scheduled to be performed on such multibeam antennas using the sixth Japanese Engineering Test Satellite (ETS-VI), to be launched in 1993. The configuration of the ETS-VI antenna system[1] is shown in Fig. 1. Each of the main reflectors is connected to the satellite main body via its deployment mechanisms at two points. Each of the antenna subreflectors is mounted on the tip of support booms and driven by an antenna pointing mechanism (APM). The support booms are connected to the antenna tower at two points in the same way as the main reflector.

A block diagram of the antenna pointing control system of ETS-VI is shown in Fig. 2. Besides a conventional attitude control system (ACS) for coarse antenna pointing, an antenna driving control system (ADCS) is incorporated for fine pointing that achieves an antenna pointing accuracy of 0.015 deg. According to our pointing error budget, the pointing deviation caused by the antenna main reflectors should be <0.001 deg, and antenna pointing control accuracy should be <0.002 deg. In the diagram, the dynamics of the large antenna main reflectors and support booms are very important in terms of the design of the antenna pointing control system.

Two significant problems exist in deriving main reflector and support boom dynamics. One is how to derive the dynamics of a satellite with a closed-loop flexible structure. The other is to clarify the dynamics of a flexible structure with a movable rigid body mounted at its tip. Some useful derivation methods have been reported[2,3]; however, in Likins' method,[2] the dynamics of a flexible structure with multiple connection points is unclear because the interface between the flexible and rigid bodies is limited to only one. In Bodley's method,[3] although the whole motion of a system including a closed loop could be numerically simulated, the equations of motion could not be analytically obtained. Therefore, this paper first describes how to incorporate the flexibility of those structures mentioned into coupling coefficients based on the data from a NASTRAN model of a flexible body. Second, those coupling coefficients are numerically and experimentally verified. Finally, using the dynamics derived, their influence on the antenna pointing capabilities of the ETS-VI system is evaluated.

Dynamics of Multipoint Connected Flexible Structures

The antenna main reflector for ETS-VI shown in Fig. 3 is connected at multiple points to the satellite main body for structural stability. In this configuration, the main reflector, two support booms (including deployment mechanisms), and the satellite main body constitute a closed loop. The rigidity of the deployment mechanism greatly influences the eigenfrequency of the whole antenna structure. Therefore, it is important to derive the dynamics of a satellite with a flexible antenna reflector including deployment mechanisms.

Deriving the dynamics of this configuration is considered to be difficult because, as pointed out before, Likins' method[2] depends on a single connection point between flexible and rigid bodies, and the origin of the coordinate of the flexible body is located on an interface between them. On the other hand, DISCOS,[3] which uses Bodley's method, can simulate the motion of a system with a closed loop, but cannot indicate an analytical equation of that motion. Therefore, the author used Bodley's method to clarify the dynamics of the system and to express the coupling coefficients.

Derivation of the Dynamics

First, the satellite system is separated into two systems and an equation of motion is derived for each. One equation is for the flexible antenna reflector and the other is for the rigid main body. Then, using the constraints at the connection points concerning velocity and angular velocity, the two equations are combined.

The equations of motion of the flexible antenna main reflector (with the origin of the coordinate at the middle point of A and B) are

$$I_A\dot{\omega}_A + m_A(r_{Ag}\times)\dot{v}_A + H_A\ddot{\xi}_A = T_A \tag{1}$$

$$m_A(r_{Ag}\times)^T\dot{\omega}_A + m_A\dot{v}_A + P_A\ddot{\xi}_A = F_A \tag{2}$$

$$H_A^T\dot{\omega}_A + P_A^T\dot{v}_A + \ddot{\xi}_A + \omega_{\mathrm{AMA}}^2\xi_A = Q_A \tag{3}$$

P_A and H_A can be calculated using the mass matrix and mode shape obtained by NASTRAN modal analysis.

The equations of motion of the satellite main body (with the origin of the coordinate at the center of gravity of main body) are

$$I_S\dot{\omega}_S + (\omega_S\times)I_S\omega_S = T_S \tag{4}$$

$$m_S\dot{v} + (\omega_S\times)m_Sv_S = F_S \tag{5}$$

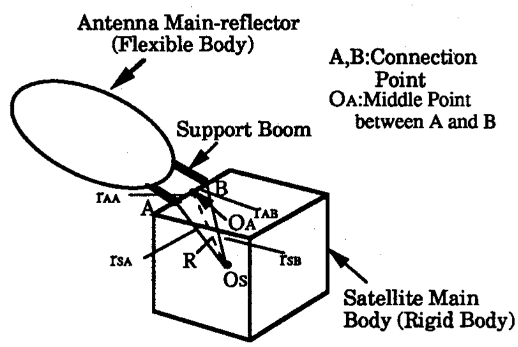

Fig. 3 Connection between antenna main reflector and satellite main body.

Constraint at connection points A and B is expressed as

$$\omega_S = C_A^S[\omega_A + \sigma(i)\dot{\xi}_A] \tag{6}$$

$$v_S + (\omega_S \times)r_{Si} = C_A^S[v_A + (\omega_A \times)r_{Ai} + \phi(i)\dot{\xi}_A] \tag{7}$$

At each connection point, $\phi(i)$ and $\sigma(i)$ are equal to zero when the flexible antenna reflector connects to the rigid satellite main body. Therefore, Eqs. (6) and (7) are expressed as

$$\omega_S = C_A^S \omega_A \tag{6'}$$

$$v_S + (\omega_S \times)r_{Si} = C_A^S[v_A + (\omega_A \times)r_{Ai}] \tag{7'}$$

Equation (6′) is the same for the angular velocity at both connection points A and B. It can be also shown that Eq. (7′) represents the same condition concerning velocity at connection points. Using Eq. (6′) and the geometrical relation in Fig. 3 expressed as

$$r_{SA} - C_A^S r_{AA} = r_{SB} - C_A^S r_{AB} = R \tag{8}$$

Equation (7′) of point A can be transformed into Eq. (7′) of point B as

$$\begin{aligned} v_S + (\omega_S \times)r_{SA} &= C_A^S[v_A + C_S^A(\omega_S \times)C_A^S r_{AA}] \\ v_S - C_A^S v_A &= (\omega_S \times)(r_{SA} - C_A^S r_{AA}) \\ &= (\omega_S \times)(r_{SB} - C_A^S r_{AB}) \\ v_S + (\omega_S \times)r_{SB} &= C_A^S[v_A + C_S^A(\omega_S \times)C_A^S r_{AB}] \end{aligned}$$

It follows that the two constraint equations with respect to the two connection points are one and the same and the constraint equation can be expressed as

$$b_1[\omega_S^T, v_S^T]^T + b_2[\omega_A^T, v_A^T, \dot{\xi}_A^T]^T = 0 \tag{9}$$

$$b_1 = \begin{bmatrix} E & 0 \\ (-R\times) & E \end{bmatrix}, \qquad b_2 = \begin{bmatrix} -C_A^S & 0 & 0 \\ 0 & -C_A^S & 0 \end{bmatrix} \tag{10}$$

Using Lagrange multipliers, the constraint equations are combined as

$$\begin{bmatrix} I_S\dot{\omega}_S + (\omega_S \times)I_S\omega_S - T_S \\ m_S\dot{v}_S + (\omega_S \times)m_S v_S - F_S \end{bmatrix} = b_1^T \begin{bmatrix} \lambda_1 \\ \lambda_2 \end{bmatrix} \tag{11}$$

$$\begin{bmatrix} I_A\dot{\omega}_A + m_A(r_{Ag}\times)\dot{v}_A + H_A\ddot{\xi}_A - T_A \\ m_A(r_{Ag}\times)^T\dot{\omega}_A + m_A\dot{v}_A + P_A\ddot{\xi}_A - F_A \\ H_A^T\dot{\omega}_A + P_A^T\dot{v}_A + \ddot{\xi}_A + \omega_{\mathrm{AMA}}^2\xi_A - Q_A \end{bmatrix} = b_2^T \begin{bmatrix} \lambda_1 \\ \lambda_2 \end{bmatrix} \tag{12}$$

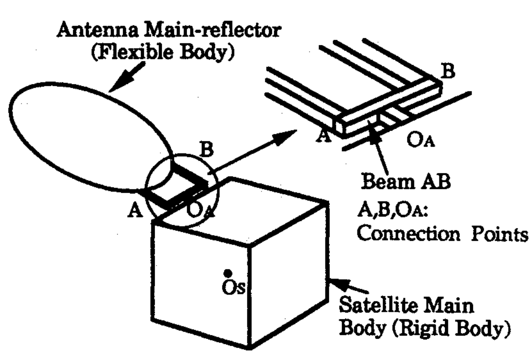

Fig. 4 Validation model for modal angular momentum (conventional method).

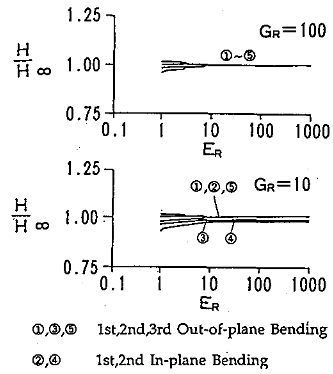

Fig. 5 Modal angular momentum with respect to O_A.

By eliminating the Lagrange multipliers and neglecting higher order terms, equations of motion of the whole system are obtained as follows:

$$\begin{aligned} &J\dot{\omega}_S + m_A[(R + C_A^S r_{Ag})\times]\dot{v}_S + [C_A^S H_A + (R\times)C_A^S P_A]\ddot{\xi}_A \\ &\quad - [C_A^S T_A + (R\times)C_A^S F_A + T_S] = 0 \end{aligned} \tag{13}$$

$$\begin{aligned} &-m_A[(R + C_A^S r_{Ag})\times]\dot{\omega}_S + (m_S + m_A)\dot{v}_S + C_A^S P_A\ddot{\xi}_A \\ &\quad - (F_S + C_A^S F_A) = 0 \end{aligned} \tag{14}$$

$$\begin{aligned} &[C_A^S H_A + (R\times)C_A^S P_A]^T\dot{\omega}_S + (C_A^S P_A)^T\dot{v}_S + \ddot{\xi}_A \\ &\quad + \omega_{\mathrm{AMA}}^2\xi_A - Q_A = 0 \end{aligned} \tag{15}$$

Based on Eqs. (13–15), the coupling coefficient between translational motion and flexible structure vibration Ω_{AT} and the one between the rotational and vibrational motion of flexible structure Ω_{AR} can be shown as

$$\Omega_{AT} = C_A^S P_A,\ \Omega_{AR} = C_A^S H_A + (R\times)C_A^S P_A \tag{16}$$

Suppose that O_A' is located from O_A at distance r, then Ω_{AR}, which uses P_A' and H_A' with respect to O_A', proves to be independent of the origin of the coordinate of the antenna main reflector using the parallel axis theorem of modal angular momenta[4] as follows:

$$\begin{aligned} &C_A^S H_A' + [(R + C_A^S r)\times]C_A^S P_A' \\ &= C_A^S[H_A - (r\times)P_A] + [(R + C_A^S r)\times]C_A^S P_A \\ &= H_A + (R\times)C_A^S P_A \end{aligned} \tag{17}$$

Numerical Verification

As a validation, the modal angular momenta of the two NASTRAN models shown in Figs. 3 and 4 are numerically compared. The latter model connects to the satellite main body at one point via beam AB. Both momenta are calculated with respect to the origin of the satellite main body with $C_A^S = E$.

Figure 5 shows that those momenta H in the latter model converge to momenta H_∞ of the former model for all vibration modes as the relative Young modulus E_R and the relative Modulus of rigidity G_R of beam AB increase. This means that, if the mass of beam AB is zero and the beam is completely rigid, then the modal angular momenta of both models must be the same. Thus, it follows that momenta can be calculated regardless of the number of connection points.

Experimental Verification

For an experimental verification, the transfer function of the apparatus shown in Fig. 6 was measured. The apparatus consisted of a rotating table with a two-point connected aluminium beam and was floated by a magnetic bearing. The rotational angle was measured by a laser measurement system. Input torque was generated by the rotor reaction of a dc motor. Table 1 lists the major structural parameters of the apparatus. Equations of motion of the apparatus with respect to the rotational axis can be expressed as follows:

$$I_e\ddot{\theta}_e + \omega_e\ddot{\xi}_e = T_e \tag{18}$$

$$\ddot{\xi}_e\omega_e^2\xi_e + \Omega_e\ddot{\theta}_e = 0 \tag{19}$$

Also, the transfer function between the input torque and the rotational angle can be expressed as follows:

$$\frac{\theta_e}{T_e} = \frac{s^2 + \omega_e^2}{I_e[(1 - \Omega_e^2/I_e)s^2 + \omega_e^2]} \tag{20}$$

In these equations, the coupling coefficient Ω_e can be calculated only by the data of NASTRAN modal analysis. The measured transfer function was then compared with the analytical one in Fig. 7. The experimental graph agrees well with the analytical one with only a slight discrepancy due to measurement error of the moment of inertia of the rotating table.

It is clarified that 1) the effect of the flexibility of a flexible structure on a rigid body is independent of the number of connection points when that structure is rigidly connected to the rigid body, and 2) this effect can be calculated regardless of the position of the origin of the coordinate in the flexible structure and can be expressed by modal momentum and modal angular momentum based on a NASTRAN mathematical model. Therefore, the effect of multiple connection points, including the deployment mechanism, can be precisely incorporated into the equation.

Dynamics of a Flexible Structure with a Movable Rigid Body at Its Tip

As for the ADCS dynamics, the rotational motion of the driven subreflector is considered to couple the rotational motion of the main body directly as well as through the vibration of the support boom. However, reports on this type of dynamics have apparently not been published to date. Therefore, by using the same method, all dynamics are derived, including the vibration of the support boom and the motion of the main body.

Table 1 Parameters of experimental apparatus

I_e, kgm^2	ω_e, rad/s	Ω_e, $\sqrt{\text{kgm}^2}$
0.293	4.54	0.414

Table 2 Parameters of experimental apparatus

I_A, kgm^2	γ	Φ_{AS}', rad	Ω_{AS}, m
5.0×10^{-4}	0.08	3.116	1.686
ω_{ASB}, rad/s	Ω_{AS}, $\sqrt{\text{kgm}^2}$	C, kgm^2	
3.12	1.56×10^{-3}	1.846	

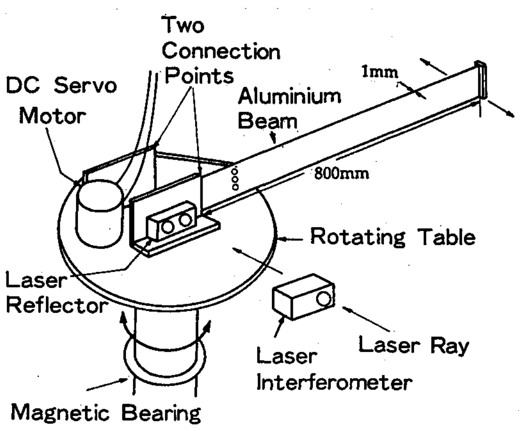

Fig. 6 Experimental apparatus (multiconnected main reflector model).

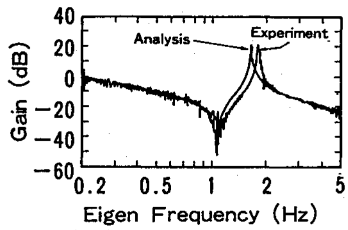

Fig. 7 Comparison of transfer function (multiconnected main reflector model).

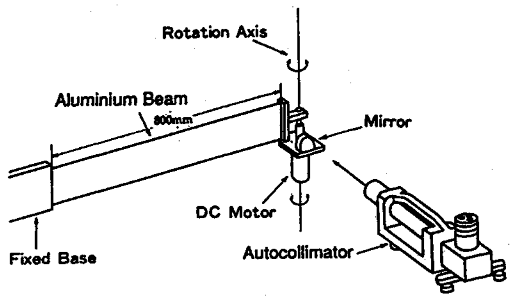

Fig. 8 Experimental apparatus (driven subreflector model).

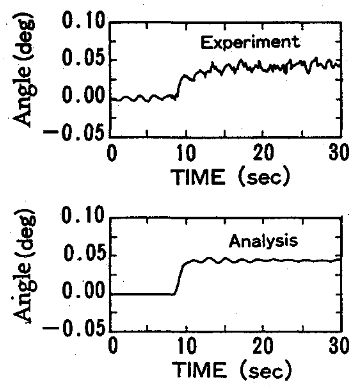

Fig. 9 Comparison of step response (driven subreflector model).

Derivation of the Dynamics

A whole system consists of three bodies. The first is a rigid satellite main body including an antenna tower. The second is a flexible antenna support boom attached to the antenna tower via a deployment mechanism. The third is a rigid antenna subreflector mounted on the support boom and rotationally driven by the APM.

There are two constraint equations. One is the completely rigid connection condition between the satellite main body and the antenna support boom; the other is the one having three rotational degrees of freedom between the antenna support boom and the antenna subreflector.

In the same way as in the previous section, the independent equations of the three bodies and two constraint equations are combined by using Lagrange multipliers. Then, by eliminating multipliers and neglecting higher terms, the whole equations of motion of the system are derived. The two-dimensional equations are expressed as

$$I_S\ddot{\theta}_S + \Omega_{ASB} + \ddot{\xi}_{ASB} + \Omega_R\ddot{\theta}_{AS} = T_S \tag{21}$$

$$I_{AS}\ddot{\theta}_{AS} + \Omega_R\theta_S + \Omega_{AS} + \ddot{\xi}_{ASB} + k_p\theta_{AS} = T_{AS} \tag{22}$$

Table 3 Critical parameters of antenna support boom

	Nominal case	Worst case	Test data
ζ_{ASB}	0.01	0.007	0.013
Φ'_{AS}, rad	−0.157	−0.204	0.160
Φ_{AS}, m	0.060	0.078	0.060

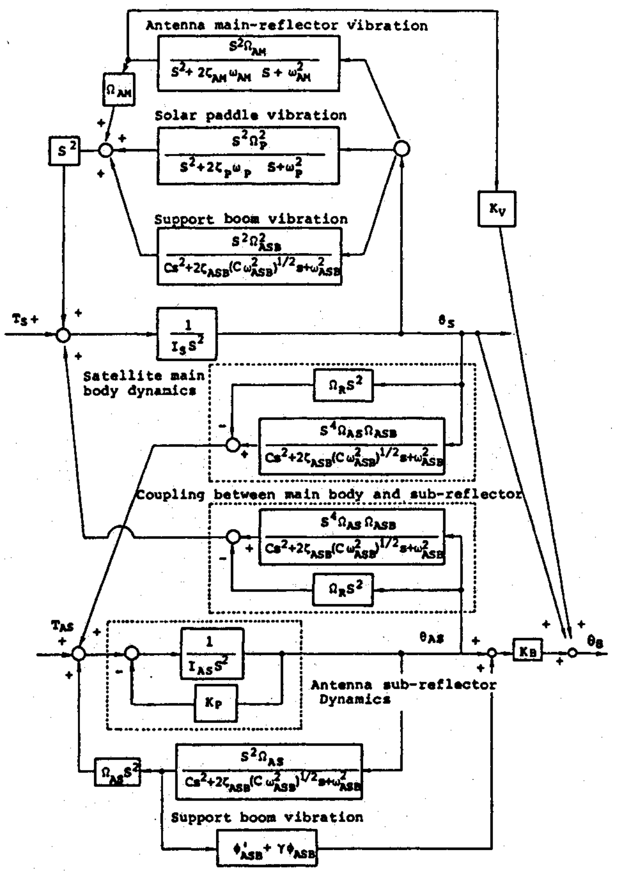

Fig. 10 Block diagram of whole dynamics of antenna point control system.

$$C\ddot{\xi}_{ASB} + 2\zeta_{ASB}\sqrt{C\omega_{ASB}^2}\,\dot{\xi}_{ASB} + \omega_{ASB}^2\xi_{ASB}$$

$$+ \Omega_{AS}\ddot{\theta}_{AS} + \Omega_{ASB}\ddot{\theta}_S = 0 \tag{23}$$

$$\theta_B = K_B\{\theta_{AS} + (\gamma\Phi_{AS} + \Phi_{AS})\xi_{ASB}\} + \theta_S \tag{24}$$

Equation (21) represents the attitude motion of the satellite main body, Eq. (22) represents the rotational motion of the driven subreflector, and Eq. (23) represents the vibration of the flexible antenna support boom. Equation (24) represents the total amount of antenna pointing directions.

The direct coupling of the subreflector with the satellite main body Ω_R can easily be understood based on the conservation law of the angular momentum of a rigid body. The coefficient Ω_{ASB}, the coupling between the rigid motion of the main body and the vibration of the antenna support boom, which takes into account the effect of a driven subreflector, can be calculated by modal angular momenta in the same way as in the previous section. In this calculation, it can be assumed that the subreflector is fixed on the support boom at any given driving angle. On the other hand, the coefficient Ω_{AS}, the coupling between the relative rotational motion of the driven subreflector and the vibration of the support boom, is expressed as relative modal angular momentum about the driving axis by the rigid subreflector. Of the three coefficients just mentioned, Ω_{AS} is newly derived and therefore needs experimental verifications.

Experimental Verification

For verification, the experimental apparatus shown in Fig. 8 was used. It is composed of an aluminium beam with a movable rigid body attached to its tip and fixed on a massive base. The movable rigid body is composed of a mirror and a small dc motor. The rotational angle is measured by an autocollimator. Input torque is generated by the rotor reaction of the dc motor. Table 2 lists major structural parameters. For this configuration Eq. (21) and terms concerning θ_S and $\ddot{\theta}_S$ are dropped.

A step response comparison is adopted rather than a transfer function comparison due to the narrow measurement range of the autocollimator. In the analysis, only a first vibrational mode is taken into account. The experimental graph nearly agrees with the analytical one as shown in Fig. 9. The difference is caused by a deviation in the initial condition and the vibration of the dc motor itself and the higher frequency vibration of the support boom. The experimental result is stable and has the same offset against a step command of 0.05 deg and the same vibration frequency.

ETS-VI Antenna Pointing Evaluation

Using the equations of motion clarified, all of the dynamics of the ETS-VI antenna pointing control system are derived as shown in Fig. 10.

From the viewpoint of the dynamics of the antenna pointing control system, variations due to changes in structural parameters are important because ACS and ADCS design is based on nominal dynamics given by nominal structural parameters. Variations in dynamics are most probably caused by uncertainties in the flexibility of the antenna main reflector and the antenna support boom.

Therefore, using flexibility data based on NASTRAN models of those structures, pointing deviation due to main reflector vibration and gain change of the ADCS due to a 30% variation in some critical structural parameters of the antenna support booms are evaluated in Figs. 11 and 12. The critical parameters used in the analysis are listed in Table 3.

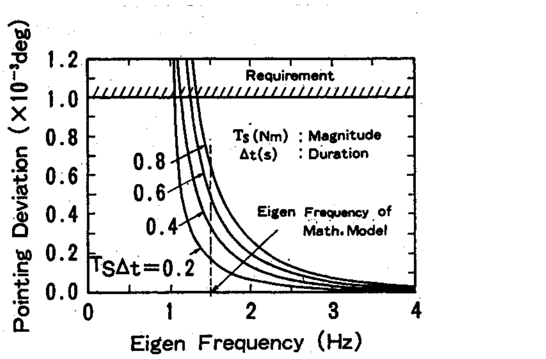

Fig. 11 Pointing deviation and rigidity of antenna main reflector (3.5 m diam).

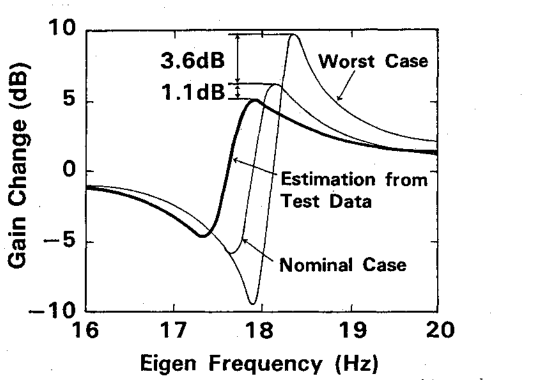

Fig. 12 Resonating of subreflector structures.

It was found that 1) pointing deviation due to 3.5-m main reflector vibration is far less than 0.001 deg under a reasonable disturbance torque of 1 Nm for a duration of 0.4 s and 2) the amount of gain jump in the worst case is expected to be 3.6 dB more than that in the nominal case, which can be compensated for by the gain margin of the control system. Based on the component test data, the most probable gain jump proved to be 1.1 dB less than that of the nominal case, which is well within the gain margin of the control system.

Conclusion

Flexible dynamics, which are peculiar to the configuration of the ETS-VI antenna pointing control system, have been derived and their validity was theoretically and experimentally confirmed and the following conclusions were reached:

1) The coupling of a flexible body with a rigid one is irrelevant to the number of connection points and the coupling coefficient can be calculated only by modal momentum and modal angular momentum based on a NASTRAN model of the flexible body when it is rigidly connected to the rigid one.

2) The coupling of a driven rigid body with the flexible one can be expressed as relative modal angular momentum about the driving axis.

Using the equation of motion derived, the author evaluated the influence of the change in the dynamics of the ETS-VI antenna system on antenna pointing capabilities (i.e., the pointing deviation due to main reflector vibration and the gain change of the subreflector dynamics).

Acknowledgments

The author would like to thank Kozo Morita, Executive Manager of the Communication Satellite Technology Laboratory; Isao Ohtomo, Research Group Leader of the same laboratory; and Yoichi Kawakami, of the same laboratory, for their valuable guidance and suggestions during discussions pertaining to this study.

References

[1]Kawakami, Y., Hojo, H., and Ueba, M., "Design of an On-Board Antenna Pointing Control System for Communication Satellites," AIAA Paper 88-4306, Aug. 1988.

[2]Likins, P. W., "Dynamics and Control of Flexible Space Vehicles," NASA TR 32-1329, 1970.

[3]Bodley, C. S., "Digital Computer Program for the Dynamic Interaction Simulation of Controls and Structure (DISCOS)," NASA TP-1219, 1978.

[4]Hughes, P. C., "Modal Identities for Elastic Bodies with Application to Vehicle Dynamics and Control," *Journal of Applied Mechanics*, Vol. 47, 1980, pp. 177–184.